

Time correlations and $1/f$ behavior in backscattering radar reflectivity measurements from cirrus cloud ice fluctuations

K. Ivanova,¹ T.P. Ackerman,² E.E. Clothiaux,¹
P.Ch. Ivanov,³ H.E. Stanley,³

and

M. Ausloos⁴

¹ Department of Meteorology
Pennsylvania State University
University Park, PA 16802, USA

² Pacific Northwest National Laboratory
U.S. Department of Energy, Richland, WA 99352, USA

³ Center for Polymer Studies, Boston University
Boston, MA 02215, USA

⁴ SUPRAS and GRASP, University of Liège
Sart Tilman B5, B-4000 Liège, Euroland

November 21, 2018

Abstract

The state of the atmosphere is governed by the classical laws of fluid motion and exhibits correlations in various spatial and temporal scales. These correlations are crucial to understand the short and long term trends in climate. Cirrus clouds are important ingredients of the atmospheric boundary layer. To improve future parameterization of cirrus clouds in climate models, it is important to understand the cloud properties and how they change within the cloud. We study correlations in the fluctuations of radar signals obtained at isodepths of *winter* and *fall* cirrus clouds. In particular we focus on three quantities: (i) the backscattering cross-section, (ii) the Doppler velocity and (iii) the Doppler spectral width. They correspond to the physical coefficients used in Navier Stokes equations to describe flows, i.e. bulk modulus, viscosity, and thermal conductivity. In all cases we find that power-law time correlations exist with a crossover between regimes at about 3 to 5 min. We also find that different type of correlations, including $1/f$ behavior, characterize the top and the

bottom layers and the bulk of the clouds. The underlying mechanisms for such correlations are suggested to originate in ice nucleation and crystal growth processes.

1 Introduction

Ice research spans a broad range of subjects, including studies of extremely complex phase diagrams [Mishima and Stanley, 1998], and phase transition modelling [Huckaby et al. 2000], hot topics as still seen recently [Putrino and Parrinello, 2002] in *ab initio* calculations, or in various properties, such as the dielectric constant [Gingle and Knasel, 1975] or acoustic emission features [Weiss and Grasso, 1997] during crack propagation. In clouds, ice crystals appear in a variety of forms and shapes, depending [Rogers, 1976; Heymsfield and Platt, 1984] on the formation mechanism and the atmospheric conditions. In cirrus clouds, at temperatures lower than about -40° C ice crystals form and exist as mainly nonspherical particles [Petrenko and Whitworth, 1999].

In air transport, ice covering of airplane wings is also known to be very annoying. Moreover high altitude clouds, found above ca. 4 km including stratosphere cirrus [Tabazadeh et al., 1997] at > 20 km, play an important role in regulating the energy budget [Wallace and Hobbs, 1977] of the earth atmosphere system through their interaction with solar and terrestrial radiation [Stephens, 1990]. Their impact on the climate and weather systems at various time and space scales is not well understood. Recent studies suggests that the water vapor itself rather than the *greenhouse gases* could be the culprit in the global warming [Maurellis, 2001; Rosenfeld and Woodley, 2001]. Indeed due to the presence of water everywhere and the ability to change its state from, say, its frozen form at the poles to its liquid and vapor states in the atmosphere, the water is an effective transfer energy medium around the globe. No need to say that the description of ice crystal motions in clouds, and the cloud motion itself imply solving Navier-Stokes equations containing physical coefficients not well determined at this time.

The radiative properties of the ice particles are important ingredients of the parameterization algorithms [Heymsfield and Platt, 1984; Sundqvist et al., 1989; Zhang and McFarlane, 1995; McFarquhar and Heymsfield, 1997; Zurovac-Jevtic, 1999] used in radiative transfer schemes of cirrus clouds in large-scale climate models. The question is still open on how cirrus radiative transfer properties might be predicted given their (actually) roughly known microphysical characterization [Smith and Del Genio, 2001]. Therefore, it is essential that correlations between the structure of cirrus clouds and the radiative properties be better understood. An interesting study on composite cirrus morphology and correlations with temperature and large-scale vertical motion has been also conducted in e.g. [Mace, 1997].

Because of the vertical extent, ca. from about 4 to 14 km and higher, and the

layered structure of such clouds, one way of obtaining some information about their properties is using ground-based remote sensing instruments. (Satellites can also be used [Liou *et al.*, 2002]). Experienced workers at airport radar sites have some *feeling* about ice cloud content. However a scientific inner cloud morphology investigation consists in searching for the statistical properties of radio wave signals backscattered from the ice crystals present in the cloud. Backscattered signals received at the radar receiver antenna are known to depend on the ice mass content and on the particle size distribution [Atlas *et al.*, 1995]. Ice particles can induce modifications in the radar signals which lead to fluctuations in (i) the backscattering cross section, (ii) the Doppler velocity and (iii) the Doppler spectral width. The motivation for our study is to identify properties of the inner structure of the cirrus clouds through a statistical analysis of the fluctuations of such measured signals. This is a first step toward including these statistics in parameterization schemes of cirrus clouds in large-scale climate models (see references quoted supra) or in short scale Navier-Stokes equation solutions. It is of interest to examine the *time* correlations in the backscattered signals not only on the boundary layers, i.e. at the top and bottom of the cloud, but also at several levels within the cloud, because of the extended vertical structure of cirrus clouds. Analysis of *spatial* correlations in vertical direction will be considered in a future study.

Due to the nonlinear physics laws governing the phenomena in the atmosphere, data series of atmospheric quantities are usually *non-stationary*. Therefore a mere study based on the power spectrum only would be incomplete, if not misleading. New techniques have been recently developed that can systematically eliminate trends in the data and thus reveal some intrinsic dynamical properties such as fluctuation correlations that are very often masked by nonstationarities. There have been indeed a large number of studies on long-range power-law correlations in time series [Kantz and Schreiber, 1997; Brockwell and Davis, 1998; Malamud and Turcotte, 1999; Schreiber, 1999] in many research fields such as biology [Stanley *et al.*, 1993; Hausdorff *et al.*, 1997; Ivanov *et al.*, 1996, 1999; Mercik *et al.*, 2000; Ashkenazy *et al.*, 2001], finance [Mantegna and Stanley, 1995; Vandewalle and Ausloos, 1997; Ausloos and Ivanova, 1999] meteorology and climatology [Koscielny-Bunde *et al.*, 1993, 1998; Davis *et al.*, 1996; Ivanova *et al.*, 2000, 2002; Ausloos and Ivanova, 2001; Bunde *et al.*, 2001; Peters *et al.*, 2002]. Some of us have already examined long-range time correlations in nonstationary atmospheric signals of the liquid water path [Ivanova *et al.*, 2000] and water vapor path [Ivanova *et al.*, 2002] in stratus clouds, as well as in large-scale meteorological signals like the Southern Oscillation Index [Ausloos and Ivanova, 2001].

We pursue the analysis of millimeter wave cloud radar data [Mace *et al.*, 1997, 1998], hereby collected from observations during two consecutive *winter* days, i.e. Jan. 26 and 27, 1997 and one *fall* day, i.e. Sept. 26, 1997 at the Southern Great Plains site of the Atmospheric Radiation Measurements (ARM) program. Mace *et al.*, [1998] have derived the microphysical properties of cir-

rus layer from surface based millimeter radar and infrared radiometer data. Mace et al. [1998] have developed techniques for retrieving cirrus cloud boundaries, ice water content, crystal effective radius, and number concentration from reflectivities combined with atmospheric emitted radiance interferometer downwelling radiances and have applied the algorithm to almost two years of MMCR data (11/96-5/98) at the Atmospheric Radiation Measurement (ARM) Program Southern Great Plains (SGP) Cloud and Radiation Testbed (CART) site. Here we analyze the statistical properties of the three quantities: (i) the backscattering cross section per unit volume, (ii) the Doppler velocity and (iii) the Doppler spectral width, obtain their time correlations, and give some physical interpretation.

First, let $\mathcal{N}(D, \vec{r})$ be the distribution function for the number of particles per unit volume; each particle is supposed to have a characteristic size D when located at \vec{r} ; let $\sigma(D)$ be the backscattering cross section of particles with such a characteristic size D . Then the total backscattering cross section (BCS) per unit volume [Clothiaux et al., 1995] is

$$\eta(\vec{r}) = \int_D \sigma(D) \mathcal{N}(D, \vec{r}) dD. \quad (1)$$

Leaving aside technical factors, the power received at the radar receiver antenna is proportional to $\eta(\vec{r})$

$$P(\vec{r}) \sim \frac{\eta(\vec{r})}{r^2}. \quad (2)$$

Due to the particle movement, frequency shifts w_m , called Doppler shifts, appear in the scattered signal

$$w_m = -\frac{4\pi v_m}{\lambda_c}, \quad (3)$$

where m is the index of the particle that moves with its so called fall velocity v_m and λ_c is the wavelength of the sounding signal [Clothiaux et al., 1995].

The radar is equipped with signal processing units, which strip off the carrier frequency and create signal voltages. By applying a Fourier transform over the raw voltage time series one can obtain the power density S_m at each velocity v_m [Clothiaux et al., 1995]. From Eq. (3) one can express the power density as a function of velocities rather than as a function of frequency. As such, the power density S_m at each velocity v_m is directly related to the total backscattering cross-section of all particles moving with a radial velocity v_m with respect to the radar. Let \tilde{S}_m be the normalized power density spectra at velocity v_m , i.e.

$$\tilde{S}_m = \frac{S_m}{\sum_1^{\mathcal{N}} S_m}, \quad (4)$$

where \mathcal{N} corresponds to the number of particles in the resolution volume.

The radar signal processor units store the mean power-weighted radial velocity within the resolution volume as

$$\langle v \rangle = \sum_{m=1}^{\mathcal{N}} v_m \tilde{S}_m, \quad (5)$$

which is usually referred to as the Doppler velocity.

The standard deviation of the power-weighted velocities about the mean is also stored

$$\sigma_v^2 = \sum_{m=1}^{\mathcal{N}} [v_m - \langle v \rangle]^2 \tilde{S}_m \quad (6)$$

and is called the Doppler spectral width. These will be related to physical properties later on, in Section III.

We study the signals of the backscattering cross section η , the Doppler velocity $\langle v \rangle$ and the Doppler spectral width σ_v^2 at different levels within the vertical structure of cirrus clouds. We apply the detrended fluctuation analysis (DFA) method [Peng *et al.*, 1994] to characterize the correlations in these signals. The DFA method is suited to accurately quantifying power-law correlations in noisy nonstationary signals with polynomial trends [Peng *et al.*, 1994; Vandewalle and Ausloos, 1998; Hu *et al.*, 2001; Chen *et al.*, 2002]. The advantage of the DFA method over conventional methods, such as the power spectrum analysis, is that it avoids the spurious detection of apparent long-range correlations that are an artifact of the nonstationarity (related to linear and higher order polynomial trends in the data). The DFA method has been tested at length by some of us on controlled time series that contain long-range correlations superposed on a (nonstationary) trend. Of note is a recent independent review of fractal fluctuation analysis methods which determined that DFA is one of the most robust methods [Taqqu *et al.*, 1995].

Briefly, the DFA method involves the following steps:

(i) The signal time series $\xi(i)$, $i = 1, 2, \dots, N$ is integrated, to “mimic” a random walk

$$y(n) = \sum_{i=1}^n (\xi(i) - \langle \xi \rangle), \quad (7)$$

where $\langle \xi \rangle = \sum_{i=1}^N \xi(i) / N$.

(ii) The integrated time series is divided into boxes of equal length, τ .

(iii) In each box of length τ , a least squares line is fit to the data (representing the *trend* in that box). The y coordinate of the straight line segments is denoted by $z(n)$.

(iv) The integrated time series, $y(n)$, is detrended by subtracting the local trend, $z(n)$, in each box.

(v) For a given box size τ , the characteristic size of fluctuation $F(\tau)$ for this integrated and detrended time series is calculated:

$$F(\tau) = \sqrt{\frac{1}{\tau} \sum_{n=k\tau+1}^{(k+1)\tau} [y(n) - z(n)]^2} \quad k = 0, 1, 2, \dots, \left(\frac{N}{\tau} - 1\right) \quad (8)$$

(vi) The above computation is repeated over all time scales (box sizes τ) to provide a relationship between $F(\tau)$ and the box size τ (i.e. the size of the window of observation).

A power law relation between the average root-mean-square fluctuation function $F(\tau)$ and the size of the observation window indicates the presence of so called scaling [Ma, 1976], i.e. when the fluctuation correlations can be characterized by a scaling exponent α , the self-similarity parameter, as in

$$F(\tau) \sim \tau^\alpha. \quad (9)$$

For uncorrelated random walk fluctuations the $F(\tau)$ function scales with an exponent $\alpha = 1.5$ [Schroeder, 1991; Addison, 1997, Turcotte, 1997]. An exponent $\alpha > 1.5$ indicates a persistent correlated behavior in the fluctuations, while an exponent $\alpha < 1.5$ characterizes anticorrelations. In other words, if $\alpha < 1.5$, the signal increments during the nonoverlapping successive time intervals of size τ tend to be of opposite signs, so that the signal $y(n)$ has a tendency to decrease in the next time step if it has had an increasing tendency in the previous one and vice versa. The feature is called antipersistence, or there are *anticorrelations*. If $\alpha > 1.5$ the signal increments tend to have the same signs, so that $y(n)$ tends to increase in the future if it has had an increasing tendency in the past, and conversely. The feature is called *persistence*. Physically, a persistent system is going to increase its statistical mean with time as if a positive feedback dominates the system. The antipersistence expresses a tendency of the values of increments to compensate for each other; this prevents the process from blowing up or going down very fast. Such a system tends to eliminate deviations, as if there is a negative feedback. An antipersistent time series visit, on average, the mean value more often than an ordinary one; the signal is said to present *anticorrelations*. Notice that the scaling exponent α can be related to the exponent β of the power spectral density $S(f) \sim f^{-\beta}$ of such a time series $y(t)$, i.e. $\beta = 2\alpha - 1$ [Heneghan and McDarby, 2000].

There are different ways of detrending the signal: one can fit the data in a window to a linear, quadratic, cubic [Vandewalle and Ausloos, 1998] or higher degree polynomial and then study the fluctuations of the signal. Discussions on different ways of detrending a signal, including a periodic and power-law trends, can be found in Hu et al. [2001].

2 Data and Data Analysis

We analyze data collected with a millimeter wave cloud radar that operates at $34.86 \text{ GHz} \pm 200 \text{ MHz}$.¹ The radar produce measurements at four modes [Clothiaux *et al.*, 2000] that are used to obtain a best estimate to cloud signal following an interpolation procedure described in [Clothiaux *et al.*, 2000]. The radar measures the backscattering cross-section of the emitted wave per unit volume of cloud particles. Assuming that the Rayleigh approximation is valid and ice crystals are spherical particles (we are aware of the approximation) this cross section is proportional to the sixth moment of the particle size and also depends on its ice water content [Mace, 1997]. The logarithm of the backscattering cross section is called the radar reflectivity and is the quantity typically used in the field. However, because we aim at studying the fluctuations, we prefer to use the raw backscattering cross section signal.

Continuous measurements of (i) the backscattering cross section per unit volume η , (ii) the Doppler velocity $\langle v \rangle$ and (iii) the Doppler spectral width σ_v^2 are recorded with 10 s temporal resolution 24 hours a day and with a 45 m spatial vertical resolution at 512 height levels. Radar reflectivity data measured with an accuracy of 0.5 dB are shown in Fig. 1.

An order of magnitude value for the horizontal velocity at which such clouds move is 10 m/s. Therefore the volume examined at each data point can be considered to reflect the local ice content and velocity fluctuation in a fixed volume, as if the cloud is locally stable. The number of particles in the volume is assumed to be a constant during the measurements. If this is not the case, from a statistical physics point of view, one should work in a grand canonical ensemble formalism and subsequently introduce another *ad hoc* model than in [Clothiaux *et al.*, 2000].

Studies along isotherms or isobars would be of great interest. This information being missing, we have decided to cut the cloud thickness into isodepths, identifying the cloud as being between its top and its bottom layer, i.e. at which the signal level is above -45 dB. We study the time series of the three sets of measurements at certain isodepths (relative to the thickness h of the cloud), i.e. top, $0.75 h$, $0.5 h$, $0.25 h$, and bottom. These profiles are represented in Figs. 2 and 3, from which the cloud height, thickness and their time evolution can be read.

In this study in order *not* to introduce spurious time correlation effects, we avoid large data gaps within the cloud life time, e.g. the gaps observed between 9:00 and 18:00 GMT on Jan. 26, 1997. Thus we consider that the time extent of this *winter* cloud at this location was between 18:00 GMT on Jan. 26 and 06:00 GMT on Jan. 27, 1997, which amounts to 4315 data points. The *fall* cloud extends from 18:00 to 24:00 GMT on Sept. 26, 1997 which amounts to 2048 data points.

¹<http://www.arm.gov/docs/sites/sgp/sgp.html>

The time series of the backscattering cross section η , Doppler velocity $\langle v \rangle$, and Doppler spectral width σ_v^2 at the specified heights (or isodepths) within the winter cirrus cloud are plotted in Fig. 4(a-c). Results for each DFA-function $F(\tau)$ are plotted in Fig. 5(a-e). The DFA-functions are grouped depending on the profile level, i.e. they refer to the top, $0.75 h$, $0.5 h$, $0.25 h$, or the bottom of the cloud. For the fall cirrus cloud (observed at the same experimental site), the data series of the three quantities of interest have been also analyzed along the same profile levels as the winter cloud (see Fig. 6). The results from the DFA analysis at the different height levels are displayed in Fig.7(a-e).

The scaling analysis has been used performing statistical tests to find the best slopes for the fits, and the corresponding scaling regimes. Each scaling behavior is characterized by slightly different scaling exponents, α_1 and α_2 at low and large time lag τ respectively; we find a crossover at $\tau_x \simeq 3 - 5$ min for all data series and physical quantities. The values of the α -exponents for the two scaling regimes and for the three studied quantities are summarized in Table 1 and Table 2 for the winter cloud and the fall cloud. Their values, whence the clouds, can be compared with each other, from signal type to signal type, and on both sides of the crossover time lag for a given signal. The error of the estimate of each α value is thus the error of the slope and is defined as the square root of residual sum of squares divided by the number of points in the fit minus two and by the sum of squares of the deviation with respect to the mean of the time lags [Bowman and Robinson, 1987]. The correlation coefficient for all estimates is in the range between 0.992 and 0.998.

We find that the α_1 values have a maximum in the center of the cloud for both cloud cases. We note an increase of α_1 from bottom to top for the Doppler velocity of the winter cloud, while the value of α_1 is rather constant for the fall cloud. The α_1 values remain constant for the η , $\langle v \rangle$ and σ_v^2 data and for both cloud cases, and close to 1.5, except for $\langle v \rangle$ at the cloud bottom in the Jan. 26 and 27, 1997 case.²

The α_2 values are systematically close to or below 1.0, for $\langle v \rangle$ and σ_v^2 . The backscattering cross section η values fall around 1.0. The α_2 values decrease from bottom to top for $\langle v \rangle$ and σ_v^2 , but present a maximum in the fall cloud center for the η data. The α_2 values reach a smooth maximum in the center of the cloud for both $\langle v \rangle$ and σ_v^2 data. The α_2 values reach a maximum in the center of the cloud for the η , $\langle v \rangle$ and σ_v^2 data and so in both cloud cases, though all these values are quite close to 1.0.

Thus, scaling exponents at the top of the cloud seem to have usually a lower value as compared to that in the bulk of the cloud, - *except for* $\langle v \rangle$. This could be due to a physical effect or arise from the instrumental noise contribution: at

²The short-range correlations may be influenced by the interpolation procedure that produces the best estimate to cloud signal from the four modes measurements of the millimeter wave radar. The current interpolating procedure is complicated [Clothiaux et al., 2000] and mimics the signal from the four modes in a systematic but non-uniform way.

such heights the real signal may be low as compared to the instrumental noise.³

To check the robustness of the results it is essential to perform a test on surrogate data [Schreiber, 1999; Schreiber and Schmitz, 2000]: we randomly shuffled the amplitudes of (i) the backscattering cross section per unit volume η , (ii) the Doppler velocity $\langle v \rangle$ and (iii) the Doppler spectral width σ_v^2 signals for winter and fall clouds. It is known [Viswanathan et al., 2002] that the fat tailed distributions are thought to be caused by long-range volatility correlations. Destroying all correlations by shuffling the order of the fluctuations, is known to cause the fat tails almost to vanish. We have found that the long-range correlations do vanish in surrogate data as seen from the DFA-functions plotted in Figs. 8 and 9 and Tables 3 and 4. This, together with an excellent systematic in the root mean square linear fit correlation coefficients, leads to put substance to the results found here above.

3 Discussion

Four main points seem to need some emphasis and bring newly interesting results:

(I) We find that DFA-functions $F(\tau)$ for all radar backscattering time series exhibit a crossover at about 4 min. We observe a *different scaling* behavior for the backscattering cross section η , the Doppler velocity $\langle v \rangle$ and the Doppler spectral width σ_v^2 between the top of the cloud from the bulk, and from the bottom, especially for large time scales. Short time range (< 4 min) scaling of η is *completely uncorrelated* with $\alpha_1 \approx 1.5$. Long-range correlations of η , $\langle v \rangle$ and σ_v^2 are quite similar (within error bars) for the bulk of the cloud with $\alpha_2 \approx 0.90$ for $\langle v \rangle$ and σ_v^2 and $\alpha_2 \approx 1.00$ for η . Such α -exponents (or $\beta = 1$) characterize a special physical phenomenon of interest [Schroeder, 1991], that is $1/f$ noise [Shlesinger, 1987; Weismann, 1988; Shlesinger and West, 1988; West and Shlesinger, 1989].

(II) Cirrus cloud temperature measurements with radiosondes show that the temperature within the cloud field usually varies smoothly between about -43° C and -33° C. Spontaneous freezing is thought to occur at temperatures colder than about -40° C. Assuming therefore that kinetically driven *homogeneous nucleation* is the primary formation mechanism at these temperatures [Kiang et. al, 1971; Sassen and Dodd, 1988; Tabazadeh et al., 1997a, 1997b] supercooled liquid water drops are thus seen to nucleate (and die rapidly) in water-saturated updrafts.

(III) However beside the $\alpha = 1.5$ value, i.e. indicating no correlation at all in the signal fluctuations at short time ranges, thus suggesting a birth and death (nucleation) process, the scaling difference at the crossover, to a $1/f$ process, suggests propagation effects in the cirrus cloud at long time scales, similar to growth and percolation features. The Doppler velocity measurements of the

³[http : //www.arm.gov/docs/instruments/static/mmcr.html](http://www.arm.gov/docs/instruments/static/mmcr.html)

cirrus ice particles shown in Fig. 2b suggest *updrafts* in fact, ... therefore updrafts serve as mechanisms for the aggregation of ice particles at long time ranges. The data analysis is consistent with (and somewhat proves) such an intuitive physical mechanism.

Further physical insight is obtained if we translate the η , $\langle v \rangle$ and σ_v^2 data from scattering information into usual fluid mechanics parameters. Even though the data is analyzed through a model with constant number of particles with a given (spherical) shape, and other standard approximations, nevertheless the backscattering cross section is a measure of the scattering intensity, thus clearly a measure of the ice content, in principle including particle shape, size and distribution. Therefore the η -DFA function is the direct signature of the *density-density correlation function*, i.e. the zero-wave vector structure factor. In other words, it is a measure of the cloud (fluid) *compressibility* or bulk modulus [Chaikin and Lubensky, 1995]. The $\langle v \rangle$ data leads to information about the particle velocity in the cloud, while the $\langle v \rangle$ -DFA function relates to the *velocity-velocity correlation function*. Even assuming a constant density, or a constant and identical mass for each particles, (... we are aware that this is an approximation), $\langle v \rangle$ -DFA measures the correlations in particle momenta and thus relates to the *viscosity* [Huang, 1967] of the inner cloud structure. On the contrary, *if* the particle density is not homogeneous the $\langle v \rangle$ -DFA function still has a physical meaning, i.e. it is a signature for the *diffusivity* or diffusion coefficient [Chaikin and Lubensky, 1995]. Finally the σ_v^2 data is a measure of the dissipated power due to inelastic scattering, through the velocity square [Huang, 1967], and is thus related to the (cloud) temperature. The σ_v^2 -DFA function is thus a measure of the *temperature-temperature correlation function*, whence the *thermal conductivity* [Huang, 1967].

In principle, the equations of motion for the above three physical quantities, i.e. ice density, ice crystal velocity and temperature in such cirrus clouds can be written as Navier-Stokes equations, - in terms of these three basic physical coefficients. They constitute an essential knowledge to be acquired before meaningful physical modelling. Moreover, the diffusion coefficient and the viscosity coefficient can serve as inputs in the corresponding microscopic evolution equations, i.e. the Langevin equations, with appropriate noise and drift terms.

In conclusion, the time dependence characteristics of physical quantities in cirrus clouds have been obtained. Short time range correlations of radar back scattering cross section are uncorrelated, i.e. are Brownian-like; at time lags longer than about 3 to 5 min correlations are of the $1/f$ noise type. Certain asymmetry is seen to exist from cloud top to bottom in respective scaling properties. This can be understood to be due to different mechanisms on the boundaries and in the bulk of the cloud, depending on the time scales. The data analysis leads to a consistent physical picture on the inner nonequilibrium structure, i.e. ice crystal nucleation and growth. Finally, the physical description of such cirrus clouds, is shown to be related to the bulk modulus, viscosity and thermal conductivity.

Acknowledgements

KI and HES thank NATO CLG 976148. PChI and HES thank NIH/National Center for Research Resources (Grant No. P41RR13622) and NSF for support. This research is supported in part by the Department of Energy through grant Battelle 327421-A-N4. We acknowledge using data collected at the Southern Great Plains site of Atmospheric Radiation Measurements (ARM) program.

REFERENCES

- Addison, P.S., *Fractals and Chaos*, Inst. of Phys., Bristol, 1997.
- Ashkenazy, Y., P. Ch. Ivanov, S. Havlin, C.-K. Peng, A. L. Goldberger, and H. E. Stanley, Magnitude and sign correlations in heartbeat fluctuations, *Phys. Rev. Lett.*, *86*, 1900-1903, 2001.
- Atlas, D., S.Y. Matrosov, A.J. Heymsfield, M.-D. Chou, and D.B. Wolff, Radar and radiation properties of ice clouds, *J. Appl. Meteor.*, *34*, 2329-2345, 1995.
- Ausloos, M., in: *Vom Billardtisch bis Monte Carlo - Spielfelder der Statistischen Physik*, K.H. Hoffmann and M. Schreiber, Eds. (Springer, Berlin, 2001) pp. 153-168.
- Ausloos, M., and K. Ivanova, Precise (m,k)-Zipf diagram analysis of mathematical and financial time series when m=6 and k=2, *Physica A*, *270*, 526-542, 1999.
- Ausloos, M., and K. Ivanova, Power law correlations in the Southern Oscillation Index fluctuations characterizing El Nino, *Phys. Rev. E*, *63*, 047201 (1-4), 2001.
- Bowman, A.W. and D.R. Robinson, *Introduction to statistics*, Institute of Physics Publishing, Bristol, 1987.
- Brockwell, P.J., and R.A. Davis, *Introduction to Time Series and Forecasting*, Springer Text in Statistics, Springer, Berlin, 1998.
- Bunde, A., S. Havlin, E. Koscielny-Bunde, and H.-J. Schellnhuber, Long term persistence in the atmosphere: global laws and tests of climate models, *Physica A*, *302*, 255-267, 2001.
- Chaikin, P.M., and T.C. Lubensky, *Principles of Condensed Matter Physics*,

Cambridge U.P., Cambridge, 1995.

Chen, Z., P. Ch. Ivanov, K. Hu, and H.E. Stanley, Effect of nonstationarities on detrended fluctuation analysis, *Phys. Rev E*, *65*, 041107 (1-15) 2002.

Clothiaux, E.E., T.P. Ackerman, R.T. Marchand, J. Verlinde, D.M. Babb, and C.S. Ruf, in *Proc. of the NATO ASI on Remote Sensing of Processes Governing Energy and Water Cycles in the Climate System*, Ploen, Germany, May 1-12, 1995.

Clothiaux, E.E., T.P. Ackerman, G.G. Mace, K.P. Moran, R.T. Marchand, M.A. Miller, and B.E. Martner, Objective determination of cloud heights and radar reflectivities using a combination of active remote sensors at the ARM CART sites, *J. Appl. Meteor.*, *39*, 645-665, 2000.

Davis, A., A. Marshak, W. Wiscombe, and R. Cahalan, Scale Invariance of liquid water distributions in marine stratocumulus. Part I: Spectral properties and stationarity issues, *J. Atmos. Sci.*, *53*, 1538-1558, 1996.

Gingle, A., and T.M. Knasel, Undergraduate laboratory investigation of the dielectric constant of ice, *Amer. J. Phys.*, *43*, 161-167, 1975.

Hausdorff, J.M., S.L. Mitchell, R. Firtion, C.-K. Peng, M. Cudkowicz, J. Y. Wei, and A.L. Goldberger, Altered fractal dynamics of gait: reduced stride-interval correlations with aging and Huntington's disease, *J. Appl. Physiol.*, *82*, 262-269, 1997.

Heneghan, C., and G. McDarby, Establishing the relation between detrended fluctuation analysis and power spectral density analysis for stochastic processes, *Phys. Rev. E*, *62*, 6103-6110, 2000.
62 6103 2000

Heymsfield, A.J., and C.M.R. Platt, A parameterization of the particle size spectrum of ice clouds in terms of the ambient temperature and the ice water content, *J. Atmos. Sci.*, *41*, 846-855, 1984.

Hu, K., Z. Chen, P. Ch. Ivanov, P. Carpena, and H.E. Stanley, Effect of trends on detrended fluctuation analysis, *Phys. Rev E*, *64*, 011114 (1-19) (2001).

Huang, K., *Statistical Mechanics*, J. Wiley, New York, 1967.

Huckaby, D.A., R. Pitis, A.K. Belkasri, M. Shinmi, and L. Blum, Molecular mirror images, dense ice phases, organic salts at interfaces, and electrochemical deposition: exotic applications of the Pirogov-Sinai theory, *Physica A*, *285*,

211-219, 2000.

Ivanov, P. Ch., M. G. Rosenblum, C.-K. Peng, J. E. Mietus, S. Havlin, H. E. Stanley, and A. L. Goldberger, Scaling behaviour of heartbeat intervals obtained by wavelet-based time-series analysis, *Nature*, *383*, 323-327, 1996.

Ivanov, P. Ch., A. Bunde, L. A. N. Amaral, S. Havlin, J. Fritsch-Yelle, R. M. Baevsky, H. E. Stanley, and A. L. Goldberger, Sleep-wake difference in scaling properties of the human heart, *Europhys. Lett.*, *48*, 594-600, 1999.

Ivanova, K., M. Ausloos, E.E. Clothiaux, and T.P. Ackerman, Break-up of stratus cloud structure predicted from non-Brownian motion liquid water and brightness temperature fluctuations, *Europhys. Lett.*, *52*, 40-46, 2000.

Ivanova, K., E.E. Clothiaux, H.N. Shirer, T.P. Ackerman, J.C. Liljegren, and M. Ausloos, Evaluating the quality of ground-based microwave radiometer measurements and retrievals using detrended fluctuation and spectral analysis methods, *J. Appl. Meteor.*, *41*, 56-68, 2002.

Kantz, H., and Th. Schreiber, *Nonlinear Time Series Analysis*, Cambridge U.P., Cambridge, 1997.

Kiang, C.S., D. Stauffer, G.H. Walker, O.P. Puri, J.D. Wise, Jr., E.M. Paterson, A reexamination of homogeneous nucleation theory, *J. Atmos. Sci.*, *28*, 1222-1232, 1971.

Koscielny-Bunde, E., A. Bunde, S. Havlin, H. E. Roman, Y. Goldreich, and H.-J. Schellnhuber, Indication of a Universal Persistence Law Governing Atmospheric Variability, *Phys. Rev. Lett.*, *81*, 729-732, 1998.

Koscielny-Bunde, E., A. Bunde, S. Havlin, and Y. Goldreich, Analysis of daily temperature fluctuations, *Physica A*, *231*, 393-396, 1993.

Liou, K. N., S. C. Ou, Y. Takano, J. Roskovensky, G.C. Mace, K. Sassen, and M. Poellot, Remote sensing of three-dimensional inhomogeneous cirrus clouds using satellite and mm-wave cloud radar data, *Geophys. Res. Lett.*, *29*, 14846-14857, 2002.

Ma S.K., *Modern Theory of Critical Phenomena*, Benjamin, Reading, MA, 1976.

Mace, G.G., T.P. Ackerman, E.E. Clothiaux, and B.A. Albrecht, A study of composite cirrus morphology using data from a 94-GHz radar and correlations with temperature and large scale vertical motion, *J. Geophys. Res.*, *102*, 13 581-

13 593, 1997.

Mace, G.G., T.P. Ackerman, P. Minnis, and D.F. Young, Cirrus layer microphysical properties derived from surface based millimeter radar and infrared radiometer data, *J. Geophys. Res.*, *103*, 23 207-23 216, 1998.

Malamud, B.D. and D.L. Turcotte, Self-affine time series: measures of weak and strong persistence *J. Stat. Plann. Infer.*, *80*, 173-196, 1999.

Mantegna, R.N., and H.E. Stanley, Scaling behavior in the dynamics of an economic index, *Nature*, *376*, 46-49, 1995.

Maurellis, A., Could water vapour be the culprit in global warming?, *Physics World*, *14*, 22-23, 2001.

McFarquhar, G.M., and A.J. Heymsfield, Parameterization of tropical cirrus ice crystal size distributions and implications for radiative transfer: Results from CEPEX, *J. Atmos. Sci.*, *54*, 2187-2200, 1997.

Mishima, O., and H. E. Stanley, Decompression-induced melting of ice IV and the liquid-liquid transition in water, *Nature*, *392*, 164-167, 1998.

Mercik, S., Z. Siwy, and K. Weron, What can be learnt from the analysis of short time series of ion channel recordings, *Physica A*, *276*, 376-390, 2000.

Peng, C.-K., S.V. Buldyrev, S. Havlin, M. Simons, H.E. Stanley, and A.L. Goldberger, Mosaic organization of DNA nucleotides, *Phys. Rev. E*, *49*, 1685-1689, 1994.

Peters, O., Ch. Hertlein, and K. Christensen, A Complexity View of Rainfall, *Phys. Rev. Lett.*, *88*, 018701 (1-4), 2002.

Petrenko, V.F., and R.W. Whitworth, *Physics of Ice*, Oxford University Press, New York, 1999.

Putrino, A. and M. Parrinello, Anharmonic Raman Spectra in High-Pressure Ice from Ab Initio Simulations, *Phys. Rev. Lett.*, *88*, 176401 (1-4), 2002.

Rogers, R.R., *Short Course in Cloud Physics*, Pergamon Press, New York, 1976.

Rosenfeld, D., and W. Woodley, Pollution and clouds, *Physics World*, *14*,

33-37, 2001.

Sassen, K., and G.C. Dodd, Homogeneous nucleation rate for highly supercooled cirrus cloud droplets, *J. Atmos. Sci.*, *45*, 1357-1369, 1988.

Schreiber, Th., Interdisciplinary application of nonlinear time series methods, *Phys. Rep.*, *308*, 1-64, 1999.

Schreiber, Th., and A. Schmitz, Surrogate time series, *Physica D*, *142*, 346-382, 2000.

Schroeder, M., *Fractals, Chaos and Power Laws*, W.H. Freeman and Co., New York, 1991.

Shlesinger, M.F., Fractal time and $1/f$ noise in complex systems. *Ann. NY Acad. Sci.*, *504*, 214-228, 1987.

Shlesinger, M.F., and B. J. West, $1/f$ noise versus $1/f^\beta$ noise. in: *Random Fluctuations and Pattern Growth: Experiments and Models*, eds. H. E. Stanley and N. Ostrowsky, Kluwer Academics, Boston, 1988.

Smith, S.A., and A.D. Del Genio, Analysis of aircraft, radiosonde and radar observations in cirrus clouds observed during FIRE II, *J. Atmos. Sci.*, *58*, 451-461, 2001.

Stanley, H.E., S.V. Buldyrev, A.L. Goldberger, S. Havlin, C.-K. Peng, and M. Simons, Long-range power-law correlations in condensed matter physics and biophysics, *Physica A*, *200*, 4-24, 1993.

Stephens, G.L., S.-C. Tsay, P.W. Stackhouse, Jr., and P.J. Flatau, The relevance of the microphysical and radiative properties of cirrus clouds to climate and climatic feedback, *J. Atmos. Sci.*, *47*, 1742-1754, 1990.

Sundqvist, H.E., E. Berge, and J.E. Kristiansson, Condensation and cloud parameterization studies with a mesoscale numerical weather prediction model, *Mon. Wea. Rev.*, *117*, 1641-1657, 1989.

Tabazadeh, A., E.J. Jensen, and O.B. Toon, A model description for cirrus cloud nucleation from homogeneous freezing of sulfate aerosols, *J. Geophys. Res.*, *102*, 23 2845-23 850, 1997.

Tabazadeh, A., O.B. Toon, and E.J. Jensen, Formation and implications of ice particle nucleation in the stratosphere, *Geophys. Res. Lett.*, *24*, 2007-2010,

1997.

Taqqu, M.S., V. Teverovsky, and W. Willinger, Estimators for long-range dependence: an empirical study, *Fractals*, *3*, 785-798, 1995.

Turcotte, D.L., *Fractals and Chaos in Geology and Geophysics*, Cambridge U.P., Cambridge, 1997.

Vandewalle, N., and M. Ausloos, Coherent and random sequences in financial fluctuations, *Physica A*, *246*, 454-459, 1997.

Vandewalle, N., and M. Ausloos, Extended detrended fluctuation analysis for financial data, *Int. J. Comput. Anticipat. Syst.*, *1*, 342-349, 1998.

Viswanathan, G. M., U. L. Fulco, M. L. Lyra and M. Serva, The origin of fat tailed distributions in financial time series, (arXiv: cond- mat/ 0112484 v3 3 Jan 2002)

Wallace, J.M., and P.V. Hobbs, *Atmospheric Science*, Academic Press, New York, 1977.

Weismann, M., $1/f$ noise and other slow, nonexponential kinetics in condensed matter, *Rev. Mod. Phys.*, *60*, 537-571, 1988.

Weiss, J., and J.R. Grasso, Acoustic emission in single crystals of ice, *J. Phys. Chem. B*, *101*, 6113-6117, 1997.

West, B.J., and M.F. Shlesinger, On the ubiquity of $1/f$ noise, *Int. J. Mod. Phys. B*, *3*, 795-819, 1989.

Zhang, G.J., and N.A. McFarlane, Sensitivity of climate simulations to the parameterization of cumulus convection in the Canadian Climate Centre general circulation model, *Atmos.-Ocean.*, *33*, 407-446, 1995.

Zurovac-Jevtic, D., Development of a cirrus parameterization scheme: Performance studies in HIRLAM, *Mon. Wea. Rev.*, *127*, 470-485, 1999.

Figure Captions

Figure 1 – Radar reflectivity observations on (a) Jan. 26, (b) 27, 1997 and (c) on Sept. 26, 1997 at the Southern Great Plains site of Atmospheric Radiation Measurements program.

Figure 2 – Cloud profiles at top and bottom and at 0.75, 0.5 and 0.25 of the thickness h of the *winter* cirrus cloud (Fig.1a,b) along which the backscattering

cross section, Doppler velocity and Doppler spectral width are studied.

Figure 3 – Cloud profiles at top and bottom and at 0.75, 0.5 and 0.25 of the thickness h of the *fall* cirrus cloud along which the backscattering cross section, Doppler velocity and Doppler spectral width are studied. Measurements are obtained at the Southern Great Plains site of Atmospheric Radiation Measurements program on Sept. 26, 1997 (Fig. 1c).

Figure 4 – (a) Backscattering cross section per unit volume at different relative heights to the thickness h of the cirrus cloud as measured on Jan. 26 and 27, 1997 at the Southern Great Plains site of Atmospheric Radiation Measurements program (data in Fig. 1a,b). (b) Doppler velocity (m/s). The positive spike between 20 and 22 h of the "bottom" data series is of order of 11 m/s.(not shown) at heights in the cloud shown in Fig. 2.; (c) Doppler spectral width (m/s) at heights in the cloud shown in Fig. 2.

Figure 5 – DFA-functions for backscattering cross section (circles), Doppler velocity (triangles) and Doppler spectral width (squares) at the (a) top, (b) 0.75, (c) 0.50, (d) 0.25 relative to the thickness h of the cloud, and (e) bottom of the *winter* cloud shown in Fig. 2. DFA-functions are displaced for readability. The α -values are listed in Table 1.

Figure 6 – (a) Backscattering cross section per unit volume at different relative heights to the thickness h of the cirrus cloud as measured on Sept. 26, 1997 at the Southern Great Plains site of Atmospheric Radiation Measurements program (Fig. 1c). (b) Doppler velocity (m/s) at heights in the cloud shown in Fig. 3; (c) Doppler spectral width (m/s) at different heights in the cloud shown in Fig. 3.

Figure 7 – DFA-functions for backscattering cross section (circles), Doppler velocity (triangles) and Doppler spectral width (squares) at the (a) top, (b) 0.75, (c) 0.50, (d) 0.25 relative to the thickness h of the cloud, and (e) bottom of the cloud shown in Fig. 3. DFA-functions are displaced for readability. The α -values are listed in Table 2.

Figure 8 – DFA-functions for shuffled data of: backscattering cross section (circles), Doppler velocity (triangles) and Doppler spectral width (squares) at the (a) top, (b) 0.75, (c) 0.50, (d) 0.25 relative to the thickness h of the cloud, and (e) bottom of the *winter* cloud shown in Fig. 2. DFA-functions are displaced for readability. The α -values are listed in Table 3.

Figure 9 – DFA-functions for the shuffled data of: backscattering cross sec-

tion (circles), Doppler velocity (triangles) and Doppler spectral width (squares) at the (a) top, (b) 0.75, (c) 0.50, (d) 0.25 relative to the thickness h of the cloud, and (e) bottom of the *fall* cloud shown in Fig. 3. DFA-functions are displaced for readability. The α -values are listed in Table 4.

Table 1: Values of the α_1 and α_2 -exponents from the DFA analysis of the backscattered cross section η , Doppler velocity $\langle v \rangle$ and Doppler spectral width σ_v^2 data shown in Fig. 4(a-c); *winter* cloud. The crossover α_1 to α_2 is at about 3 min. The error of the estimate of each α value is thus the error of the slope and is defined as the square root of residual sum of squares divided by the number of points in the fit minus two and by the sum of squares of the deviation with respect to the mean of the time lags [Bowman and Robinson, 1987].

position	η		$\langle v \rangle$		σ_v^2	
	α_1	α_2	α_1	α_2	α_1	α_2
top	1.36 ± 0.03	0.89 ± 0.01	1.43 ± 0.07	0.76 ± 0.01	1.24 ± 0.04	0.73 ± 0.01
0.75 h	1.41 ± 0.04	1.11 ± 0.01	1.38 ± 0.04	0.88 ± 0.01	1.36 ± 0.03	0.90 ± 0.02
0.50 h	1.62 ± 0.10	0.94 ± 0.01	1.42 ± 0.04	0.96 ± 0.01	1.35 ± 0.04	0.92 ± 0.02
0.25 h	1.43 ± 0.04	1.15 ± 0.02	1.29 ± 0.03	0.93 ± 0.01	1.31 ± 0.04	0.90 ± 0.02
bottom	1.46 ± 0.09	1.27 ± 0.03	1.09 ± 0.05	0.70 ± 0.02	1.38 ± 0.05	1.02 ± 0.01

Table 2: Values of the α_1 and α_2 -exponents from the DFA analysis of backscattering cross section η , Doppler velocity $\langle v \rangle$ and Doppler spectral width σ_v^2 data shown in Fig. 6(a-c); *fall* cloud. A crossover is observed at about 5 min.

position	η		$\langle v \rangle$		σ_v^2	
	α_1	α_2	α_1	α_2	α_1	α_2
top	1.32 ± 0.05	0.66 ± 0.04	1.34 ± 0.06	0.66 ± 0.01	1.32 ± 0.03	0.69 ± 0.03
0.75 h	1.63 ± 0.04	0.85 ± 0.05	1.14 ± 0.05	0.86 ± 0.03	1.37 ± 0.03	1.07 ± 0.05
0.50 h	1.50 ± 0.04	1.13 ± 0.04	1.14 ± 0.03	0.85 ± 0.03	1.37 ± 0.03	1.19 ± 0.05
0.25 h	1.69 ± 0.04	1.23 ± 0.04	1.31 ± 0.04	0.93 ± 0.03	1.27 ± 0.04	1.09 ± 0.03
bottom	1.36 ± 0.07	0.70 ± 0.03	1.22 ± 0.04	0.68 ± 0.03	1.22 ± 0.03	0.88 ± 0.02

Table 3: Values of the α -exponents- from the DFA analysis of the shuffled data of backscattered cross section η , Doppler velocity $\langle v \rangle$ and Doppler spectral width σ_v^2 data shown in Fig. 4(a-c); *winter* cloud. The correlation coefficient for all cases is around 0.997.

position	η	$\langle v \rangle$	σ_v^2
	α	α	α
top	0.47 ± 0.006	0.49 ± 0.006	0.51 ± 0.003
0.75 h	0.53 ± 0.004	0.53 ± 0.004	0.54 ± 0.004
0.50 h	0.52 ± 0.004	0.50 ± 0.005	0.52 ± 0.005
0.25 h	0.56 ± 0.006	0.53 ± 0.005	0.48 ± 0.006
bottom	0.49 ± 0.006	0.50 ± 0.004	0.49 ± 0.005

Table 4: Values of the α -exponent from the DFA analysis of shuffled data of backscattering cross section η , Doppler velocity $\langle v \rangle$ and Doppler spectral width σ_v^2 data shown in Fig. 6(a-c); *fall* cloud. The correlation coefficient for all cases is around 0.994.

position	η	$\langle v \rangle$	σ_v^2
	α	α	α
top	0.55 ± 0.006	0.48 ± 0.006	0.49 ± 0.005
0.75 h	0.48 ± 0.006	0.52 ± 0.007	0.52 ± 0.006
0.50 h	0.50 ± 0.007	0.51 ± 0.006	0.46 ± 0.006
0.25 h	0.49 ± 0.006	0.52 ± 0.005	0.52 ± 0.007
bottom	0.51 ± 0.010	0.51 ± 0.005	0.53 ± 0.007

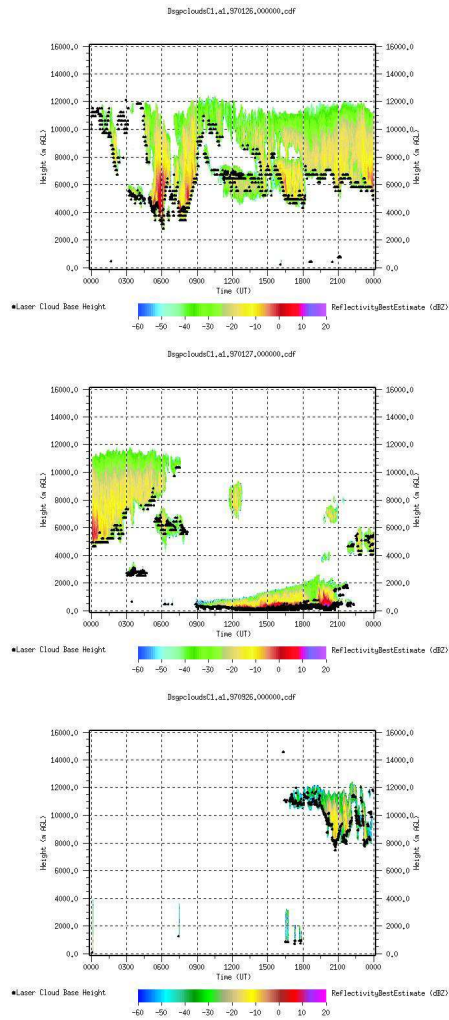


Figure 1: Radar reflectivity observations on (a) Jan. 26, (b) 27, 1997 and (c) on Sept. 26, 1997 at the Southern Great Plains site of Atmospheric Radiation Measurements program.

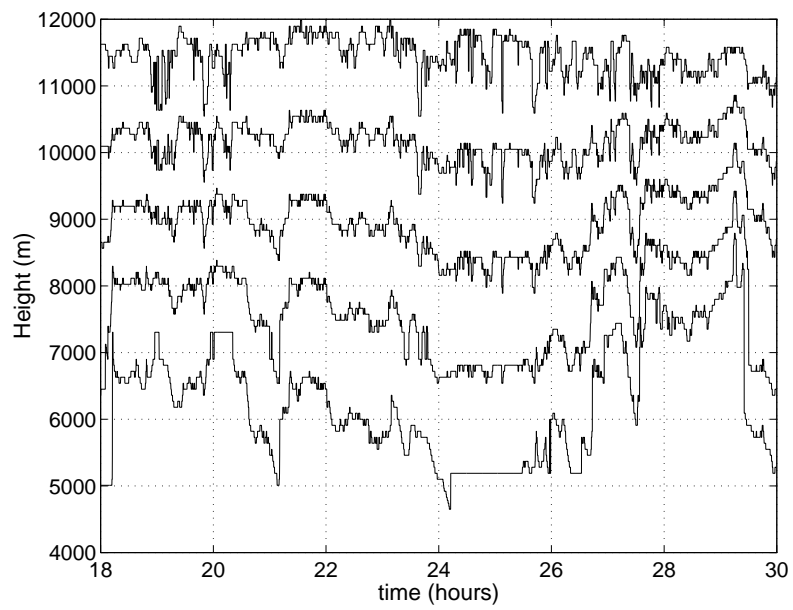


Figure 2: Cloud profiles at top and bottom and at 0.75, 0.5 and 0.25 of the thickness h of the *winter* cirrus cloud (Fig.1a,b) along which the backscattering cross section, Doppler velocity and Doppler spectral width are studied.

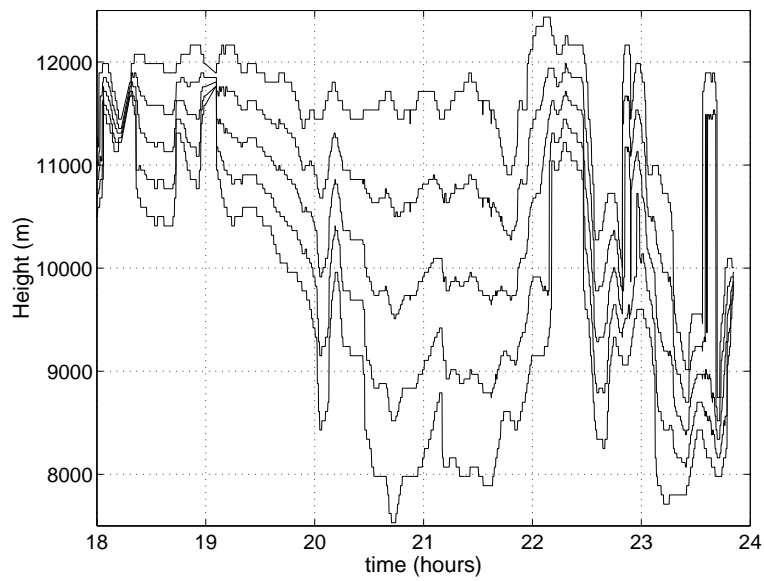


Figure 3: Cloud profiles at top and bottom and at 0.75, 0.5 and 0.25 of the thickness h of the *fall* cirrus cloud along which the backscattering cross section, Doppler velocity and Doppler spectral width are studied. Measurements are obtained at the Southern Great Plains site of Atmospheric Radiation Measurements program on Sept. 26, 1997 (Fig. 1c).

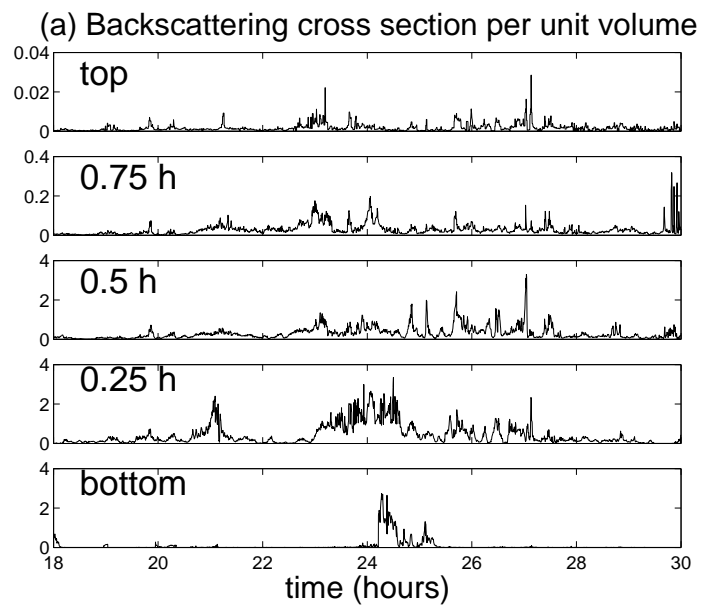


Figure 4: (a) Backscattering cross section per unit volume at different relative heights to the thickness h of the cirrus cloud as measured on Jan. 26 and 27, 1997 at the Southern Great Plains site of Atmospheric Radiation Measurements program (data in Fig. 1a,b).

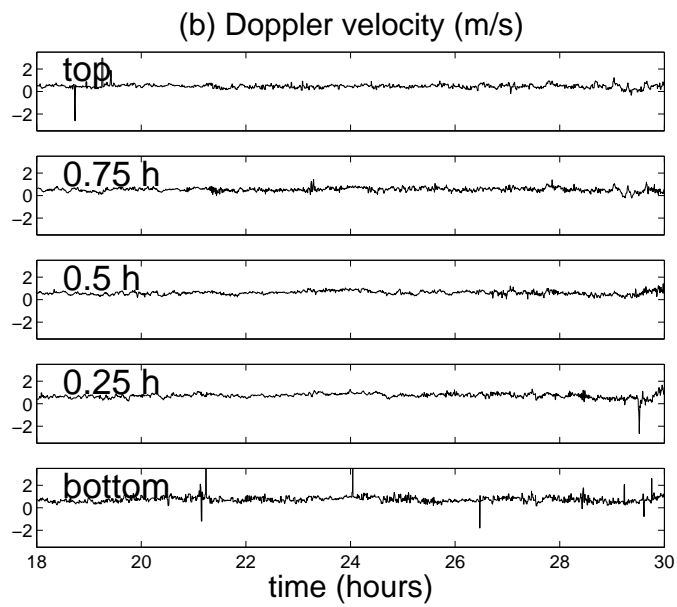


Figure 4: (b) Doppler velocity (m/s). The positive spike between 20 and 22 h of the "bottom" data series is of order of 11 m/s (not shown) at heights in the cloud shown in Fig. 2

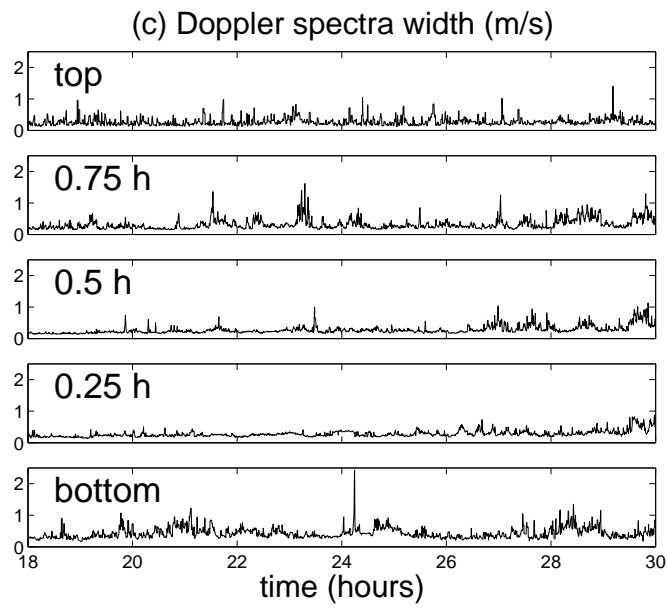


Figure 4: (c) Doppler spectral width (m/s) at heights in the cloud shown in Fig. 2

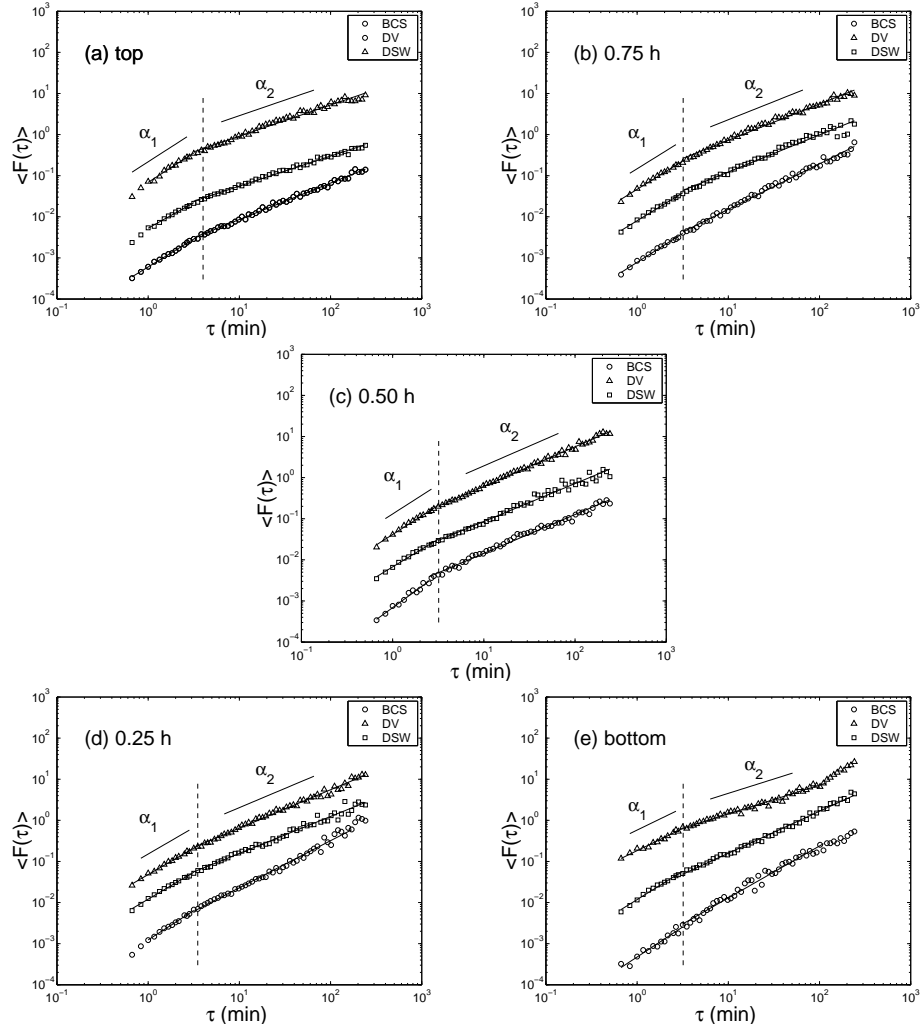


Figure 5: DFA-functions for backscattering cross section (circles), Doppler velocity (triangles) and Doppler spectral width (squares) at the (a) top, (b) 0.75, (c) 0.50, (d) 0.25 relative to the thickness h of the cloud, and (e) bottom of the *winter* cloud shown in Fig. 2. DFA-functions are displaced for readability. The α -values are listed in Table 1.

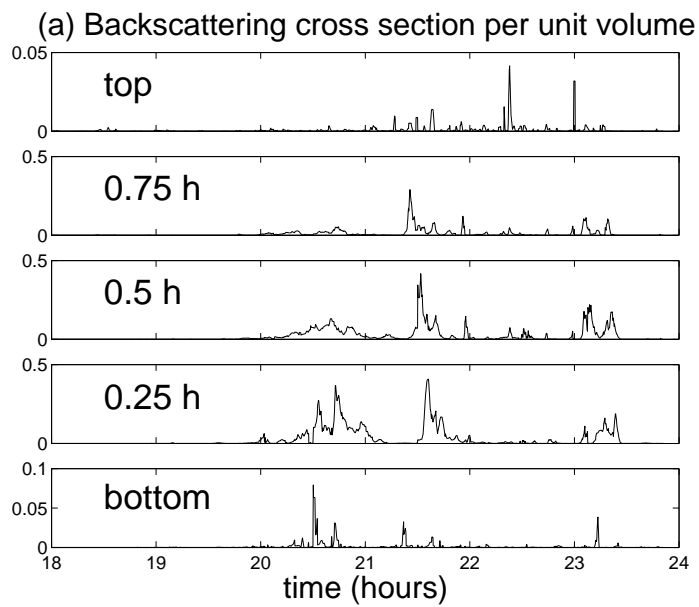


Figure 6: (a) Backscattering cross section per unit volume at different relative heights to the thickness h of the cirrus cloud as measured on Sept. 26, 1997 at the Southern Great Plains site of Atmospheric Radiation Measurements program (Fig. 1c).

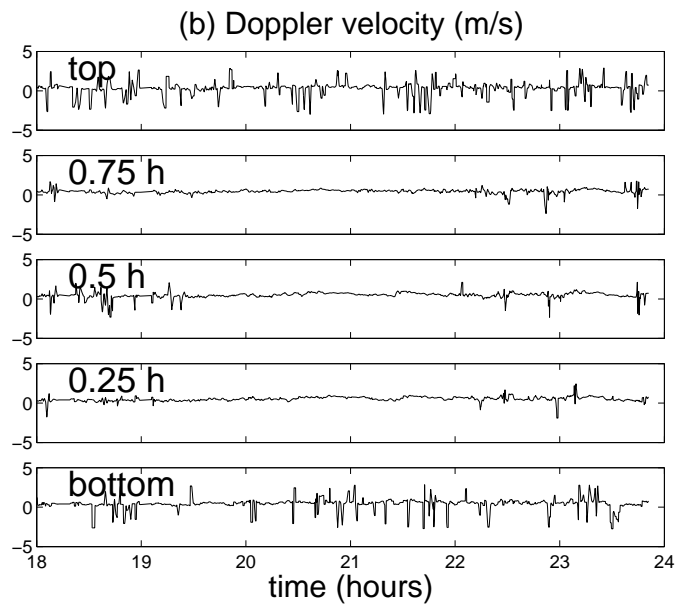


Figure 6: (b) Doppler velocity (m/s) at heights in the cloud shown in Fig. 3.

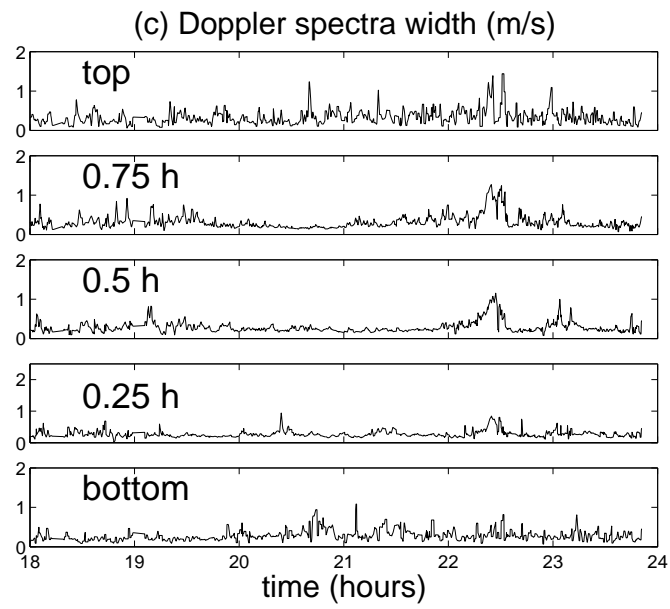


Figure 6: (c) Doppler spectral width (m/s) at heights in the cloud shown in Fig. 3.

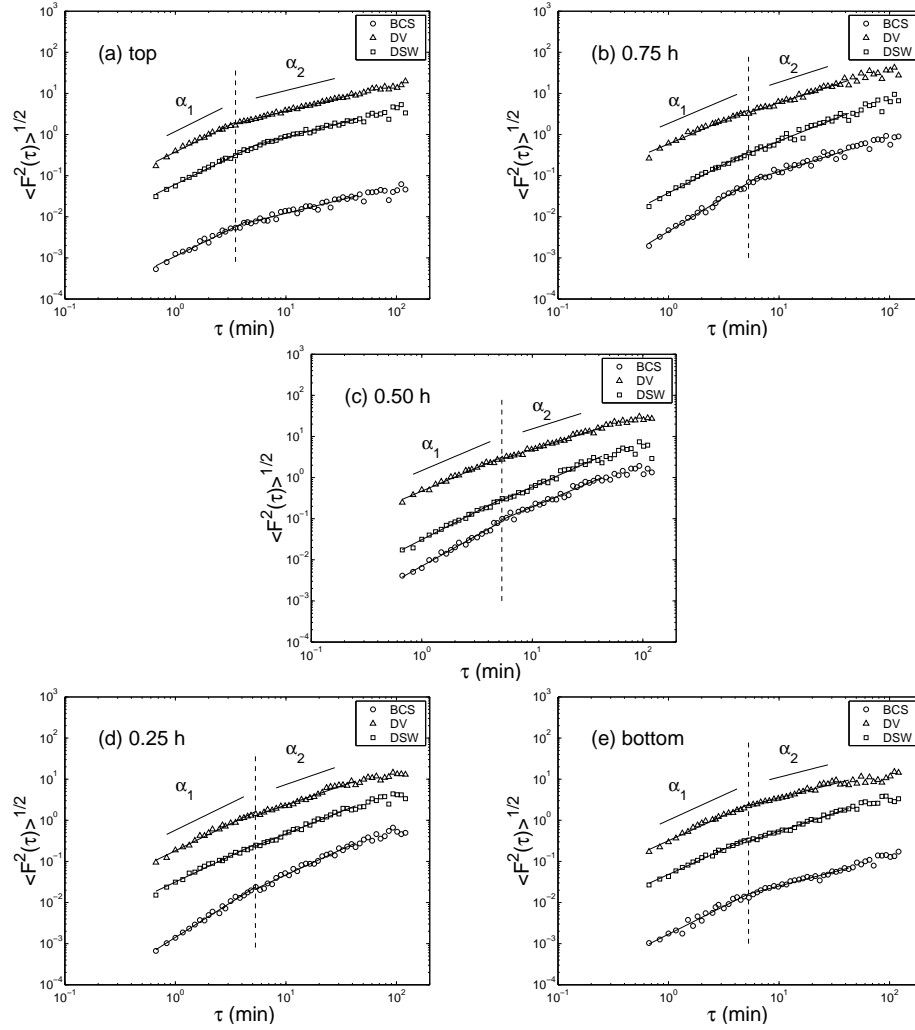


Figure 7: DFA-functions for backscattering cross section (circles), Doppler velocity (triangles) and Doppler spectral width (squares) at the (a) top, (b) 0.75, (c) 0.50, (d) 0.25 relative to the thickness h of the cloud, and (e) bottom of the cloud shown in Fig. 3. DFA-functions are displaced for readability. The α -values are listed in Table 2.

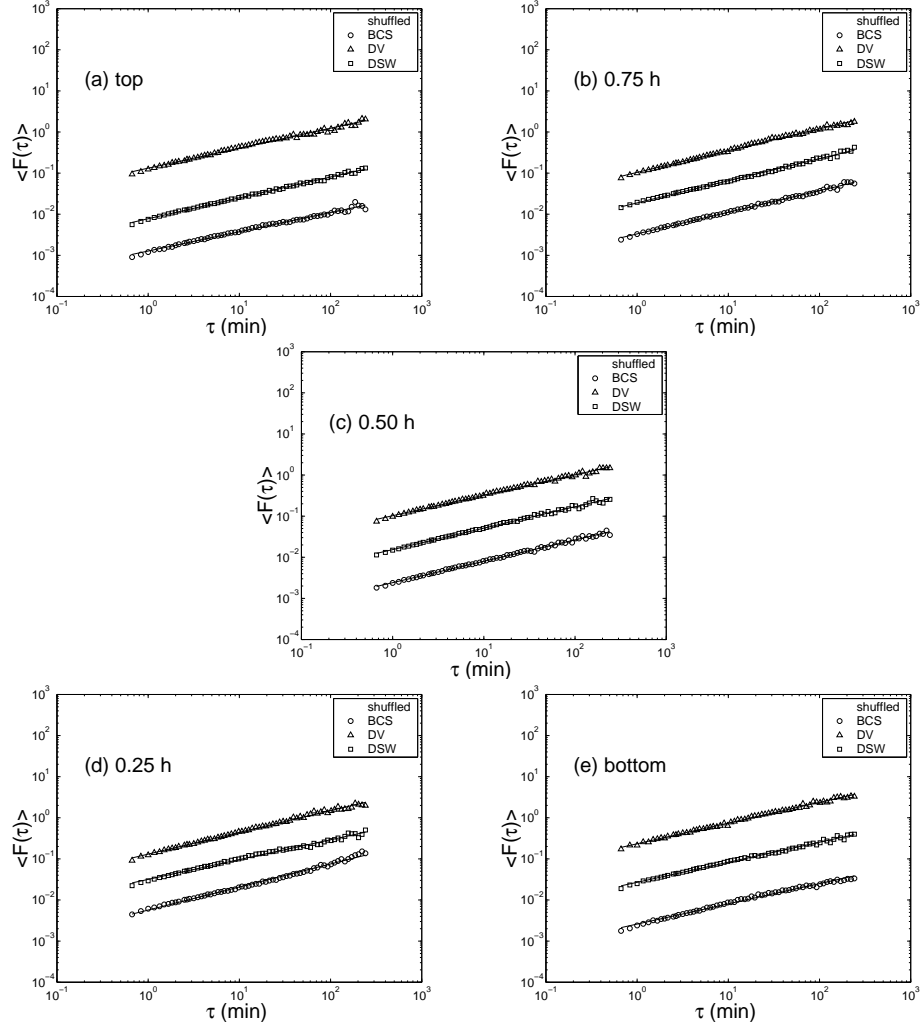


Figure 8: DFA-functions for shuffled data of: backscattering cross section (circles), Doppler velocity (triangles) and Doppler spectral width (squares) at the (a) top, (b) 0.75, (c) 0.50, (d) 0.25 relative to the thickness h of the cloud, and (e) bottom of the *winter* cloud shown in Fig. 2. DFA-functions are displaced for readability. The α -values are listed in Table 3.

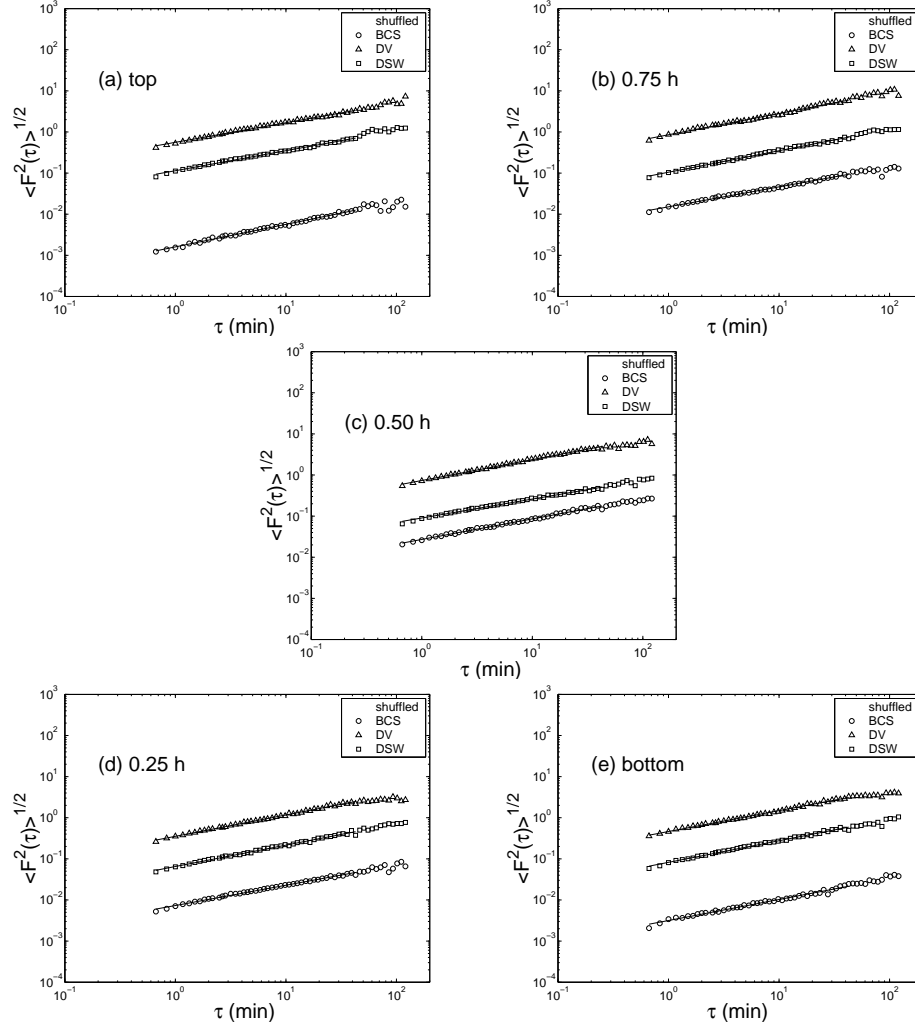


Figure 9: DFA-functions for the shuffled data of: backscattering cross section (circles), Doppler velocity (triangles) and Doppler spectral width (squares) at the (a) top, (b) 0.75, (c) 0.50, (d) 0.25 relative to the thickness h of the cloud, and (e) bottom of the *fall* cloud shown in Fig. 3. DFA-functions are displaced for readability. The α -values are listed in Table 4.